# Rapid Communication

# Changes in Glial K$^+$ Currents With Decreased Extracellular Volume in Developing Rat White Matter

**Alexandr Chvátal,[1] Thomas Berger,[2] Ivan Voříšek,[1] Richard K. Orkand,[3] Helmut Kettenmann,[4] and Eva Syková[1]***

[1]Department of Neuroscience, Second Medical Faculty, Charles University and Institute of Experimental Medicine, Prague, Czech Republic
[2]Institute of Physiology, University of Freiburg, Freiburg, Germany
[3]Institute of Neurobiology, University of Puerto Rico, San Juan, Puerto Rico
[4]Department of Cellular Neurosciences, Max-Delbrück Centre for Molecular Medicine, Berlin, Germany

Whole cell patch-clamp recordings of K$^+$ currents from oligodendrocyte precursors in 10-day-old rats (P10) and, following myelination, in mature oligodendrocytes from 20-day-old rats (P20) were correlated with extracellular space (ECS) diffusion parameters measured by the local diffusion of iontophoretically injected tetramethylammonium ions (TMA$^+$). The aim of this study was to find an explanation for the changes in glial currents that occur with myelination. Oligodendrocyte precursors (P10) in slices from corpus callosum were characterized by the presence of A-type K$^+$ currents, delayed and inward rectifier currents, and lack of tail currents after the offset of a voltage jump. Mature oligodendrocytes in corpus callosum slices from P20 rats were characterized by passive, decaying currents and large tail currents after the offset of a voltage jump. Measurements of the reversal potential for the tail currents indicate that they result from increases in [K$^+$]$_e$ by an average of 32 mM during a 20 msec 100 mV voltage step. Concomitant with the change in oligodendrocyte electrophysiological behavior after myelination there is a decrease in the ECS of the corpus callosum. ECS volume decreases from 36% (P9–10) to 25% (P20–21) of total tissue volume. ECS tortuosity $\lambda = (D/ADC)^{0.5}$, where D is the free diffusion coefficient and ADC is the apparent diffusion coefficient of TMA$^+$ in the brain, increases as measured perpendicular to the axons from $1.53 \pm 0.02$ (n = 6, mean $\pm$ SEM) to $1.70 \pm 0.02$ (n = 6). TMA$^+$ non-specific uptake (k$'$) was significantly larger at P20 ($5.2 \pm 0.6 \times 10^{-3}$s$^{-1}$, n = 6) than at P10 ($3.5 \pm 0.4 \times 10^{-3}$s$^{-1}$, n = 6). It can be concluded that membrane potential changes in mature oligodendrocytes are accompanied by rapid changes in the K$^+$ gradient resulting from K$^+$ fluxes across the glial membrane. As a result of the reduced extracellular volume and increased tortuosity, the membrane fluxes produce larger changes in [K$^+$]$_e$ in the more mature myelinated corpus callosum than before myelination. These conclusions also account for differences between membrane currents in cells in slices compared to those in tissue culture where the ECS is essentially infinite. The size and geometry of the ECS influence the membrane current patterns of glial cells and may have consequences for the role of glial cells in spatial buffering. J. Neurosci. Res. 49:98–106, 1997. © 1997 Wiley-Liss, Inc.

**Key words:** patch-clamp technique; diffusion parameters; corpus callosum; precursors; oligodendrocytes; extracellular space; development

## INTRODUCTION

Glial cells are most permeable to K$^+$, and this ion carries most of the transmembrane current when the membrane potential is displaced from the K$^+$ equilibrium

potential, $E_K$ (Orkand et al., 1966; Gardner-Medwin, 1983; Hounsgaard and Nicholson, 1983; Kettenmann et al., 1983, 1987; for review see Syková, 1992). Berger et al. (1991) studied $K^+$ currents of glial cells of the oligodendrocyte lineage in the mouse corpus callosum slice using the whole cell patch-clamp technique. They found, in slices taken at postnatal days 6–8 (P6–8), that oligodendrocyte precursor cells expressed primarily delayed rectifier and occasionally A-type outward $K^+$ currents while mature oligodendrocytes (P10–13) displayed only passive symmetrical $K^+$ currents (Berger et al., 1991). A comparison between these postnatal times is of special interest because myelination in the mouse brain begins around P11 (Sturrock, 1980). The currents of the precursor cells were similar to those described for precursor cells in culture (Sontheimer et al., 1989); in contrast to cultured cells, where symmetrical currents do not inactivate during a voltage step (Sontheimer and Kettenmann, 1988), currents in mature oligodendrocytes in slices markedly decayed during the voltage step and large tail currents appeared when the membrane potential was clamped back to the holding potential. It was suggested that this decay was due to a rapid transmembrane shift of $K^+$ (Berger et al., 1991) and its accumulation in the compact extracellular space (ECS). Cells from P6 to P8 in the slice did not exhibit either a prominent decay during a voltage step or prominent tail currents presumably because the ECS was less compact in immature animals (Lehmenkühler et al., 1993).

The ECS is the microenvironment of brain cells; it is an important communication channel between neurons, and between neurons and glial cells (Nicholson and Rice, 1991; Syková, 1991, 1992, 1997). It has been recognized in both morphological and physiological studies that the volume of the ECS in the brain is significantly larger in immature animals and progressively decreases with age (Vernadakis and Woodbury, 1965; Bondareff and Pysh, 1968; Lehmenkühler et al., 1993). The constraints for the diffusion of substances through the ECS are the volume fraction ($\alpha$)—the restricted volume of the nervous tissue which is available for diffusion—and tortuosity ($\lambda$)—the effective path length for the diffusion of particles between two points due to various obstacles in the ECS which slow down diffusion of ions and molecules in the brain. Tortuosity is a geometric factor calculated as $\lambda = (D/ADC)^{0.5}$, where D is the free diffusion coefficient and ADC is the apparent diffusion coefficient of tetramethylammonium ($TMA^+$) in the brain. In addition, the diffusion of substances can be affected by non-specific, concentration-dependent cellular uptake ($k'$) (Nicholson and Phillips, 1981; Nicholson, 1992).

In the present study, we used both patch-clamp electrophysiology and real-time measurement of ECS diffusion parameters. With this combined approach we correlated the changes in the electrophysiological properties of glial cells of the oligodendrocyte lineage with changes in ECS diffusion parameters in the rat corpus callosum during postnatal development, i.e., prior to and during myelination and maturation of nervous tissue.

## MATERIALS AND METHODS

### Preparation of Brain Slices and Electrophysiological Setup

Rat brain slices were prepared as previously described for the mouse (Berger et al., 1991). In brief, young Wistar rats (P10 and P20) were decapitated and their forebrain hemispheres cut into frontally oriented 120–170-µm-thick slices. The corpus callosum was thus cut parallel to its axonal fascicles. Slices were placed in a recording chamber mounted on the stage of an upright microscope (Zeiss, Oberkochen, Germany) and maintained at room temperature (about 20°C). The chamber was continuously perfused; the bath solution contained (in mM): NaCl 150, KCl 5.4, $CaCl_2$ 2, $MgCl_2$ 1, HEPES 5, and glucose 10. The pH was adjusted with NaOH to 7.2. The solution was gassed with $O_2$. Cell somata in the corpus callosum were visible in standard water immersion optics and could be approached by the patch electrode. Positive pressure was applied to the pipette to blow axonal bundles aside and to permit the pipette tip to be placed onto the surface of a cell soma to form a tight seal.

### Patch-Clamp Recordings

Recording pipettes were made from borosilicate capillaries (Hilgenberg, Malsfeld, Germany) with resistances around 5 M$\Omega$ and coated with Sigmacote (Sigma). The pipette contained (in mM): KCl 130, $CaCl_2$ 1, EGTA 10, $MgCl_2$ 1, and HEPES 10. $Ca^{2+}$ activity was calculated to be approximately 11 nM. The pH was adjusted with KOH to 7.2.

Membrane currents were recorded with the patch-clamp technique in the whole cell recording configuration (Hamill et al., 1981). Current signals were amplified with conventional electronics (EPC-7 amplifier, List Electronics, Darmstadt, Germany), filtered at 3 kHz, and sampled at 5 kHz by an interface connected to a computer system which also served as a stimulus generator.

### Diffusion Measurements

Diffusion measurements were performed on 12 rat pups (Wistar) from P9–10 (n = 6) and P20–21 (n = 6). Animals were anesthetized with urethane (1.6–2.5 g/kg body weight i.p.) and placed in a rat headholder. The body temperature was maintained at 36–37°C and the animals were spontaneously breathing. A hole, 2 mm in diameter, was made 2 mm lateral from the midline and 1 mm (P10)

or 2 mm (P21) caudal from the bregma (P10) and the dura was removed. The exposed brain tissue was bathed in warmed (36–37°C) artificial cerebrospinal fluid (Nicholson and Phillips, 1981).

Iontophoresis electrodes were made from double-barreled theta glass tubing (Clark Electromedical Instruments, Pangbourne, England). Double-barreled ion-selective microelectrodes (ISMs) for $TMA^+$ were prepared by a procedure previously described (for details see Syková et al., 1994). The ion-exchanger was Corning 477317 and the ion-sensitive barrel was back-filled with 100 mM $TMA^+$ chloride. The reference barrel contained 150 mM NaCl. Electrodes were calibrated using the fixed-interference method before and after each experiment in a sequence of flowing solutions. Calibration data were fitted with the Nikolsky equation to determine electrode slope and interference (Nicholson and Phillips, 1981). The shank of the iontophoresis electrode was bent, so that it could be aligned parallel to that of the ISM. An iontophoresis pipette and a $TMA^+$-ISM were glued together with tip separation of 120–170 μm. Iontophoresis parameters were: +20 nA bias current (continuously applied to maintain a constant transport number), +200 nA main current step of 60 sec duration to generate the diffusion curve.

$TMA^+$ diffusion curves were recorded with a PC-based Pentium computer and analyzed by fitting the data to a solution of the modified diffusion equation (Nicholson and Phillips, 1981) using the VOLTORO program (Nicholson, unpublished). $TMA^+$ concentrations vs. time curves were first recorded in 0.3% agar gel (Difco, Detroit, MI) made up in 150 mM NaCl, 3 mM KCl, and 0.3 mM $TMA^+$ in a cup that was placed just above the brain. The array of electrodes was then lowered through the cortex to appropriate depths (1.5–1.9 mm in P9–10 and 2.0–2.6 mm in P20–21) to reach the corpus callosum as measured in unfixed, rapidly frozen brains and confirmed by the striking difference in the diffusion parameters between gray and white matter (Lehmenkühler et al., 1993).

**Analysis of the Diffusion Measurements**

The diffusion curves in brain were analyzed to yield $\alpha$, $\lambda$, and the uptake term, $k'$ $(s^{-1})$ as previously described (Nicholson and Phillips, 1981; Syková et al., 1994). These three parameters were extracted by a non-linear curve fitting simplex algorithm operating on the diffusion curve as described by Nicholson (1992). When the experimental medium is agar, by definition, $\alpha = 1 = \lambda$ and $k' = 0$ and the parameters n (iontophoretic electrode transport number) and D ($TMA^+$ diffusion coefficient) are extracted from the curve fitting. Knowing n, D, and the distance between the electrodes (r), the parameters $\alpha$, $\lambda$, and $k'$ can be obtained when the experiment is repeated in the brain. Diffusion at P9–10 is isotropic in the x-, y-,

and z-axes (Voříšek et al., 1996), while at P20–21 diffusion is easier along the axons (x-axis) of the corpus callosum and the value of $\lambda$ is higher across the axons (y-axes). In this anisotropic case we determined $\alpha$ from the relation $\alpha = ((\lambda_y \cdot \lambda_z)/ \lambda_x^2)\alpha_x$ (for details see Rice et al., 1993). For this calculation we assume diffusion in the y- and z-axes to be equal as they are both at right angles to the direction of the axons (Voříšek et al., 1996).

Results of the experiments were expressed as the mean $\pm$ SEM. Statistical analysis of the differences between groups was evaluated using the one-way analysis of variance (ANOVA) test. Values of $P < 0.05$ were considered significant.

# RESULTS
## Voltage-Activated Currents in Glial Cells

To compare the electrophysiological properties of glial precursor cells with those of mature oligodendrocytes, we studied voltage-activated currents in glial cells from the P10 and P20 rat corpus callosum using the whole cell patch-clamp technique. These developmental stages were selected because myelination in the rat is delayed, relative to the mouse. At P10 axons in the corpus callosum are uniformly thin and naked, and myelination begins at P12 (Bjartmar et al., 1994; Bjartmar, 1996; Hamano et al., 1996).

Symmetrical 10 mV voltage steps from a holding potential $(V_h)$ of $-70$ mV elicited different current responses in oligodendrocyte precursors and mature oligodendrocytes (Fig. 1). At P10, all cells exhibited a delayed rectifier $K^+$ current (Fig. 1A, top) activated at potentials positive to $-50$ mV and inactivating during 50 msec voltage steps. The conductance of this delayed rectifying current was $3.3 \pm 0.5$ nS (n = 10, mean $\pm$ SEM). Seven of these cells expressed an additional A-type current that was isolated with a subtraction protocol as described by Connor and Stevens (1971). Conductance of A-type of $K^+$ current was $3.4 \pm 0.8$ nS (n = 7). Seven cells with a delayed rectifier $K^+$ current also expressed an inward rectifier $K^+$ current that had a voltage- and time-dependent inactivation (not shown).

The reversal potential of the currents evoked by de- and hyperpolarizing voltage steps was determined from the amplitude 3 msec after the onset of the voltage step (see dashed vertical line in Fig. 1A, top). This delay was used to avoid contaminating the ionic current with the capacitive current. Then, a current voltage (I/V) relation was constructed (Fig. 1A, bottom). In all cells the reversal potential $(V_{rev})$ was at the holding potential of $-70$ mV. As is apparent from Figure 1A, in these oligodendrocyte precursor cells only small tail currents $(I_{tail})$ were recorded when the cells were clamped back to the holding potential.

Eight glial cells in the corpus callosum of P20 rats were examined with the same stimulation protocol as described for the P10 cells. Voltage steps in the de- or
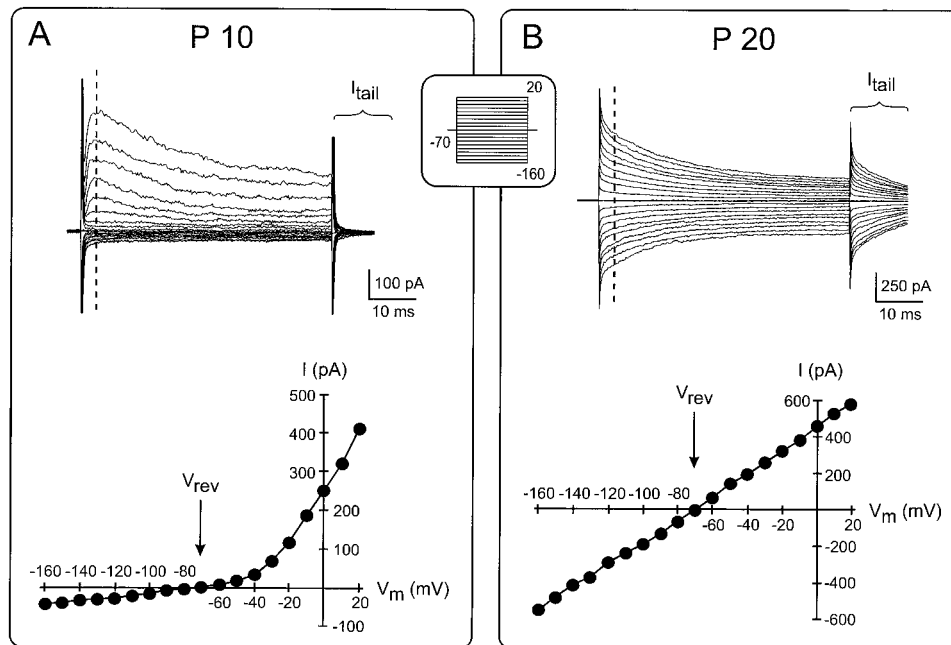
Fig. 1. Membrane properties of oligodendrocyte precursors (**A**) and mature oligodendrocytes (**B**). Membrane currents were recorded in response to voltage steps from a holding potential of $-70$ mV. To activate voltage-gated currents, the membrane was clamped for 50 msec to increasing de- and hyperpolarizing potentials (pattern of voltage commands in **inset**) ranging from $-160$ to $+20$ mV, at 10 mV increments. The corresponding current traces are superimposed. From the traces shown in A and B (top), currents (I) were measured 3 msec after the beginning of voltage pulse (dashed lines) and plotted as a function of the membrane potential ($V_m$) (bottom). The reversal potentials ($V_{rev}$), $-70$ mV in A and B, are indicated in the graphs by the arrows.

hyperpolarizing direction from a holding potential of $-70$ mV elicited in all these cells symmetrical passive non-rectifying outward and inward currents, with a linear I-V relationship (see Fig. 1B). These currents decayed during the voltage step. The reversal potential was also at the holding potential of $-70$ mV. As is readily apparent in Figure 1, in contrast to the P10 precursors, large $I_{tail}$ were recorded when the mature oligodendrocytes were clamped back to the holding potential. The properties of these tail currents were analyzed in more detail.

**Tail Current Analysis**

Tail currents were measured from a series of 10 mV test pulses from $-100$ to $+30$ mV following a depolarizing voltage step of 100 mV, i.e., by changing the holding potential from $-70$ to $+30$ mV, for 20 msec (Fig. 2, inset). $V_{rev}$ of the tail currents was determined from the current voltage (I/V) relation measured 3 msec after the onset of the test pulses. Figure 2 shows how $V_{rev}$ of the tail currents was determined for a mature oligodendrocyte. $V_{rev}$ was shifted to more positive values in mature oligodendrocytes than in oligodendrocyte precursors, even when comparable outward currents were evoked. Following this protocol, $V_{rev}$ of $I_{tail}$ was $-55.9 \pm 1.2$ mV

($n = 7$) in precursor cells and $-31.5 \pm 6.3$ mV ($n = 9$) in mature oligodendrocytes.

In another series of experiments, the effect of changing the duration or amplitude of a prepulse on the reversal potential for the membrane currents in mature oligodendrocytes was studied. Figure 3 illustrates results from one of three cells subjected to complete analysis. When the duration of the prepulse to $+30$ mV was increased from 1 to 50 msec (Fig. 3A, B), the reversal potential of $I_{tail}$ became more positive as the duration increased. When the amplitude of the 20 msec prepulse was varied from $+5$ to $+100$ mV (Fig. 3C), the reversal potential also shifted to more positive values. In another set of experiments, the outward tail currents after a 100 mV hyperpolarizing 20 msec prepulse to $-170$ mV were studied. After this step the reversal potential of the tail currents was $-105 \pm 16$ mV ($n = 3$, Fig. 3D).

For a perfectly $K^+$-selective membrane, the membrane potential and the reversal potential for the $K^+$ current are given by the Nernst equation $V_{rev} = (RT/F)\ln([K^+]_e/[K^+]_i)$. Thus, with $[K^+]_i = 130$ mM (in the pipette) a reversal potential for the tail currents of $-56$ mV for the precursor cells indicates that $[K^+]_e = 12$ mM at the end of the 100 mV depolarizing step. In the mature
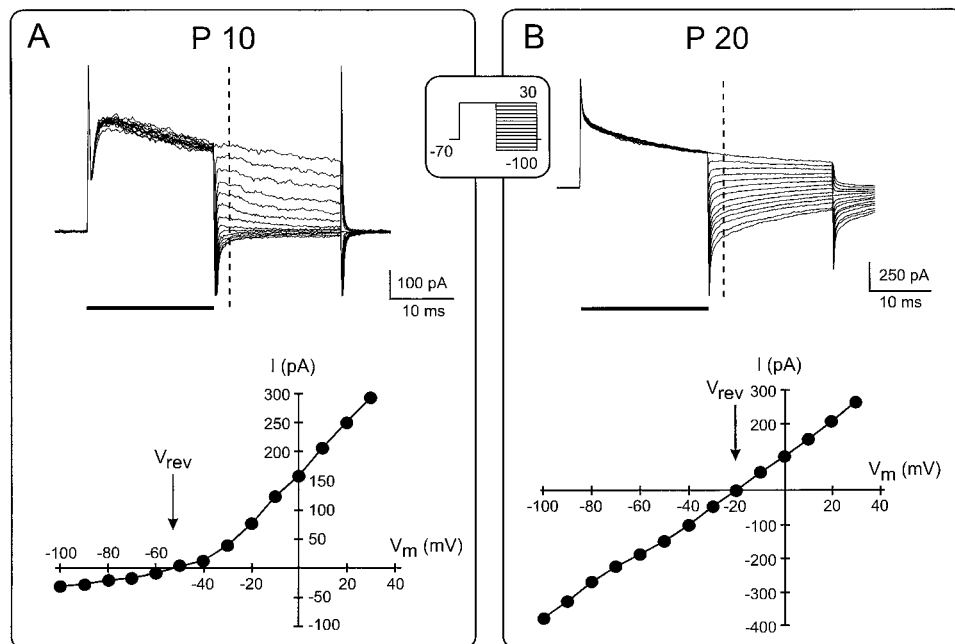
**Fig. 2.** Analysis of tail currents in oligodendrocyte precursors (**A**) and mature oligodendrocytes (**B**). The membranes of glial cells of P10 and P20 rat corpus callosum were clamped from a holding potential of $-70$ to $+30$ mV for 20 msec. After this prepulse (indicated by the bar below the traces), the membrane was clamped for 20 msec to increasing de- and hyperpolarizing potentials (pattern of voltage commands in **inset**) ranging from $-100$ to $+30$ mV, at 10 mV increments. From the traces shown in A and B (top), currents (I) were measured 3 msec after the prepulse (dashed lines) and plotted as a function of the membrane potential ($V_m$). The reversal potentials ($V_{rev}$), $-52$ mV in A and $-20$ mV in B, are indicated in the graphs by the arrows.

oligodendrocytes from P20 rats the reversal potential of $-31.5$ mV corresponds to an $[K^+]_e$ of 37 mM, while the hyperpolarizing step of 100 mV appeared to reduce $[K^+]_e$ from 5.4 to 2 mM. As the currents were comparable in oligodendrocyte precursor cells and in mature oligodendrocytes, one possible explanation for the difference is that the $K^+$, extruded during the depolarizing prepulse, is injected into a more compact ECS in corpus callosum of P20 rats than in P10 rats and thus accumulates outside the membrane to a higher concentration. To test this hypothesis, we measured the ECS diffusion parameters, i.e., volume fraction ($\alpha$), tortuosity ($\lambda$), and non-specific uptake ($k'$).

### ECS Volume Fraction, Tortuosity, and Non-Specific Uptake

After the $TMA^+$ diffusion coefficient and the transport number for the iontophoresis pipette had been determined in 0.3% agar (see Materials and Methods), the diffusion curves were recorded from the corpus callosum. The microelectrode array was either oriented along the axons (x-axis) or along the body axis at a right angle to the axons (y-axis) (Fig. 4A, inset). Superimposed on each experimental curve is the theoretical curve, plotted using the extracted parameters, $\alpha$, $\lambda$, and $k'$ (Fig. 4B). The

amplitude of the diffusion curve in the corpus callosum of the P10 rat is larger than in agar, but is much smaller than that in the P20 rat. This indicates that the ECS volume is greater in the younger animals. The calculated average diffusion parameters in P9–10 animals were, at x-axis, $\lambda = 1.49 \pm 0.03$ and $k' = 3.6 \pm 0.2 \times 10^{-3} s^{-1}$ (n = 6), and at y-axis, $\lambda = 1.53 \pm 0.02$ and $k' = 3.5 \pm 0.4 \times 10^{-3} s^{-1}$ (n = 6). In animals at P20–21 the estimates of diffusion parameters were different: at x-axis, $\lambda = 1.46 \pm 0.03$ and $k' = 5.0 \pm 0.6 \times 10^{-3} s^{-1}$ (n = 6), while at y-axis, $\lambda = 1.70 \pm 0.02$ and $k' = 5.2 \pm 0.6 \times 10^{-3} s^{-1}$ (n = 6). The volume fraction, $\alpha$, was determined using the measurements in the x- and y-axes. The derived $\alpha$ (see Materials and Methods) at P9–10 was $0.36 \pm 0.01$ (n = 6) and at P20–21 $\alpha$ was $0.25 \pm 0.01$ (n = 6). Thus, with increased age the volume fraction decreased ($P < 0.0001$) and the tortuosity increased in the y-axis ($P < 0.0001$), but was not significantly changed in the x-axis. In addition, non-specific uptake was larger in the older animals ($P < 0.02$).

The same values of $\alpha$, $\lambda$, and $k'$ as given in Figure 4B were used to construct isoconcentration plots in x-y plane representing diffusion in agar and brain. The spheres illustrate a concentration of $TMA^+$ (0.1–1.0 mM) as calculated after 60 sec of iontophoretic application in
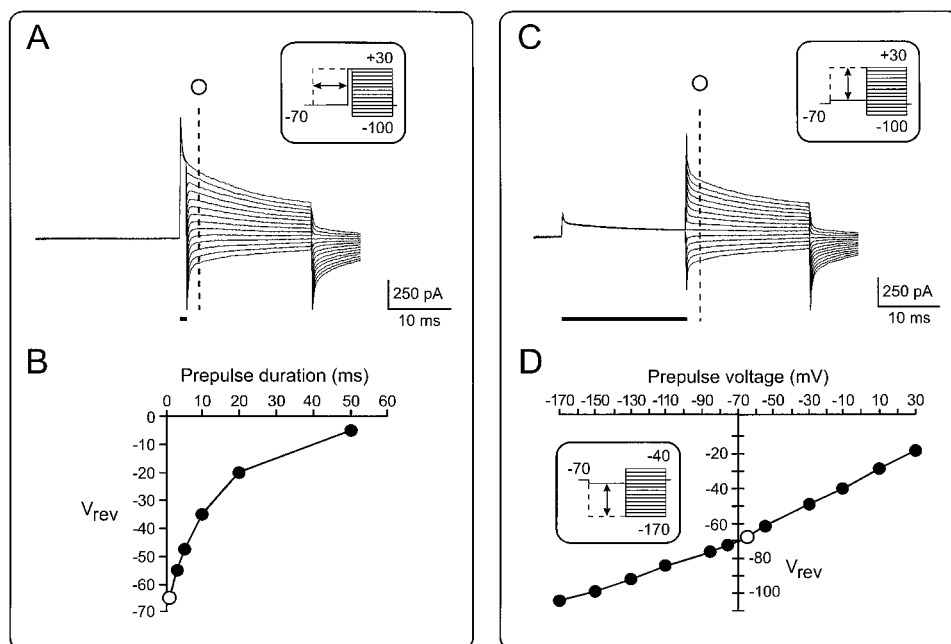
Fig. 3. Analysis of tail currents in mature oligodendrocytes after prepulses with variable time duration (**A, B**) and amplitude (**C, D**). **A:** Mature oligodendrocytes of P20 rat corpus callosum were clamped from a holding potential of −70 to +30 mV for 1 msec (top traces). After this prepulse, the membrane was clamped for 20 msec to increasing de- and hyperpolarizing potentials (pattern of voltage commands in **inset**) ranging from −100 to +30 mV, with 10 mV increments. **B:** From the traces shown in A, currents (I) were measured 3 msec after the prepulse (dashed line) and reversal potential of these currents was estimated. The reversal potentials ($V_{rev}$) in recordings with 1 msec (open circle) and 3, 5, 10, 20, and 50 msec (filled circles) prepulses are plotted in the graph as a function of the prepulse duration (indicated by the arrows in the inset in A). **C:** The membranes of mature oligodendrocytes of P20 rat corpus callosum were clamped from a holding potential of −70 to −65 mV for 20 msec (top traces). After this prepulse, the membrane was clamped to test pulses as described in A. **D:** From the traces shown in C, currents (I) were measured 3 msec after the prepulse (dashed line) and the reversal potential of these currents was estimated. The reversal potentials ($V_{rev}$) in recordings with depolarizing prepulses to −65 mV (open circle) and −55, −30, −10, +10, and +30 mV and with hyperpolarizing prepulses to −75, −85, −110, −130, −150, and −170 mV (filled circles) are plotted in the graph as a function of the prepulse voltage (indicated by the arrows in the **inset** in C and D).

agar, and in P10 and P21 animals (Fig. 4C). In agar and in P10 corpus callosum, where no anisotropy was found, isoconcentration plots are represented by circles. In contrast, in P21 corpus callosum, where tortuosity is increased across the fibers, isoconcentration plots are represented by ellipses. Isoconcentration circles in agar are significantly smaller in contrast to those in brain, because volume fraction is 100% and tortuosity is assumed to be zero. The area in which the respective $TMA^+$ concentration (0.1–1.0 mM) was reached was larger at P21 than that at P10 (Fig. 4C).

To conclude, the ECS volume fraction was about 45% larger in animals from P9–10 than in animals from P20–21. There was an increase in tortuosity perpendicular to myelinated fibers. Non-specific $TMA^+$ uptake into cells was significantly larger in P20–21 animals. The results show that the diffusion of small ions, such as $TMA^+$ and $K^+$, released from any source (e.g., iontophoretic pipette or active neuron) in the ECS is more hindered in the more mature animal.

## DISCUSSION

### Comparison of Glial Cells From Corpus Callosum Slices of Mice and Rats

In this study, we have made patch-clamp recordings from glial cells of the rat corpus callosum at two ages during postnatal development, namely at P10 and P20. These developmental stages in the rat compare to about P8 and P13 in the mouse. In the rat corpus callosum, myelination begins at about P12–14 (Bjartmar et al., 1994; Hamano et al., 1996). The electrophysiological criteria established in the study of the mouse corpus callosum (Berger et al., 1991) were used to identify the
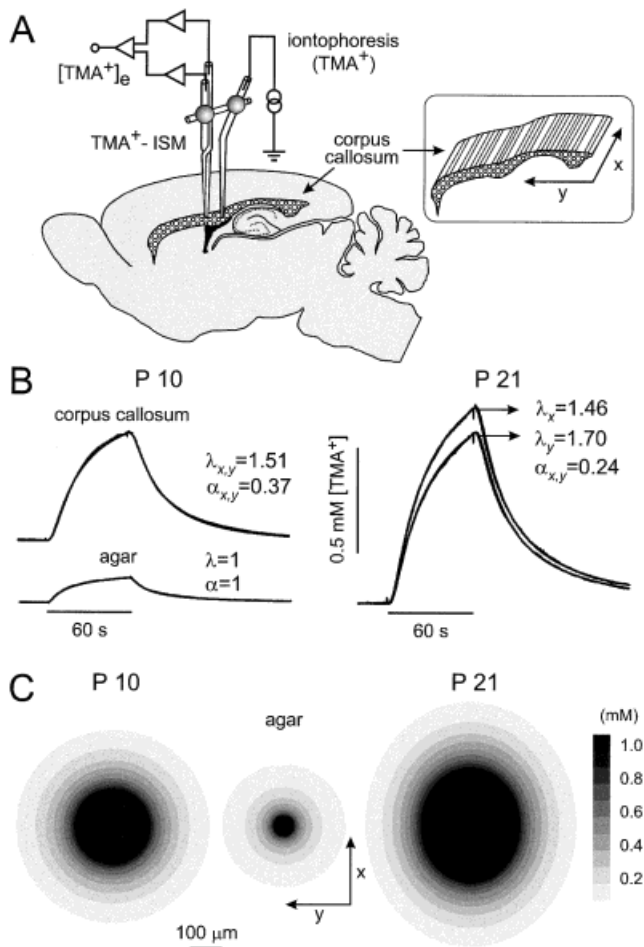
Fig. 4. Measurement of diffusion parameters in the corpus callosum from P10 and P21 rats. **A:** Schematic drawing of a section of the rat brain cut in a sagittal plane 2.0 mm lateral to the midline and the experimental setup. Three-dimensional view of a section of the corpus callosum (axes are indicated by arrows) is shown in the **inset. B:** TMA$^+$ was applied iontophoretically with the main current +200 nA for 60 sec. Curves represent recording of the TMA$^+$ concentration in the corpus callosum at x- and y-axes and in agar. Each data curve is superimposed with the theoretical diffusion curve. Note that there is no difference between curves at x- and y-axes at P10, while such difference was found in corpus callosum at P21 and represents the anisotropic diffusion. The values of volume fraction ($\alpha$) and tortuosity ($\lambda$) are shown with each recording in the brain. The depth to which the arrays were lowered, array spacing, and the electrode transport number n were, in the P10 rat, 1.8 mm, 159 μm, and 0.203, and in the P21 rat, 2.4 mm, 161 μm, and 0.207, respectively. **C:** Two-dimensional isoconcentration plots of TMA$^+$ concentrations in agar, and in P10 and P21 corpus callosum after 60 sec of iontophoretic application. Ten gray densities represent different concentrations of TMA$^+$ from 0.1 to 1.0 mM, as shown on the scale. For further explanation see text.

rat glial cells. Mouse oligodendrocyte precursor cells, between P3 and P8, expressed a dominant delayed rectifying K$^+$ current and the same current was found in the rat at P10. In contrast to the mouse, 7 of 10 cells at P10 expressed an inward rectifier K$^+$ current. Cells from P20 rats exhibited passive decaying currents similar to mice mature oligodendrocytes at P10–13. These currents were identified as K$^+$ currents in mice as they were blocked by Ba$^{2+}$ and reversed close to the E$_K$ when tested with brief pulses (for details see Berger et al., 1991).

It appears that rat cells from P10 correspond to mouse cells at P8 and are most likely immature oligodendrocyte precursor cells, whereas rat cells from P20 correspond to mouse cells at P13 and are mature oligodendrocytes.

## Oligodendrocytes Can Rapidly Shift K$^+$ Across the Membrane

In both the mature and immature corpus callosum, under resting conditions E$_K$ measured from the membrane currents in response to an initial voltage step is the same as the holding potential ($-70$ mV, Fig. 1). This indicates that K$^+$ can readily move across the membrane and distribute according to the transmembrane voltage and the Nernst equation for K$^+$.

In mature oligodendrocytes of the rat corpus callosum, we observed characteristic inward and outward tail currents after voltage steps, previously seen in mature oligodendrocytes in the mouse. As discussed in Berger et al. (1991), these tail currents are likely caused by a change of the K$^+$ gradient (E$_K$) across the membrane during the preceding voltage step. Such steps lead to a shift in the K$^+$ gradient so that the new E$_K$ is close to the clamped membrane potential. Thus the observed changes in E$_K$ are likely to result from changes in [K$^+$]$_e$ as [K$^+$]$_i$ is controlled by the pipette solution (Frankenhaeuser and Hodgkin, 1956). Moreover, when the pipette is made positive, K$^+$ currents flowing out of the cell are matched by K$^+$ current flowing out of the pipette into the cell interior. The time course of the decay of the tail currents, which is voltage-dependent (Berger et al., 1991), reflects the time course of the K$^+$ shift across the cell membrane and thus the relationship between the intracellular and extracellular environment. For the pulse protocol used in Figure 2, the Nernst equation indicates accumulations to 12 mM K$^+$ in P10 and 37 mM in P20 corpus callosum ECS. These estimates are consistent with the observation that superfusion of the rat spinal cord slices with 55 mM K$^+$ shifted the reversal potential to $-23$ mV in precursor as well as in mature glial cells (Chvátal et al., 1995).

## ECS Volume Decreases and Tortuosity Increases After the Onset of Myelination

The diffusion parameters obtained in the present study differ in important details from a previous study in

the rat corpus callosum (Lehmenkühler et al., 1993). In the current study, the parameters for P9–10 are the same but in the older animals the volume fraction is smaller. There is an increase in tortuosity, i.e., decrease in apparent diffusion coefficient of TMA$^+$, along the fibers. In these experiments, tortuosity was evaluated by measuring the diffusion of TMA$^+$ not only in parallel to the axons as in the previous study (Lehmenkühler et al., 1993), but also across the axons. As tortuosity affects the ease of diffusion, it appears that the measurement across the axons is more sensitive to the tighter packing which accompanies myelination. To calculate the extracellular volume, Lehmenkühler et al. (1993) assumed diffusion was the same in all directions and our results show that this is not the case in myelinated white matter. Taking the anisotropy into account raises the estimate of $\alpha$ at P20–21 from 0.19 to 0.24 (see Materials and Methods). The increase in non-specific uptake of TMA$^+$ in older animals could be indicative of an increase in permeability of the cell membranes to ions.

The large ECS in developing rat brain will affect the accumulation of ions, metabolites, and neuroactive substances in the ECS. When the ECS volume fraction diminishes, any substance present in, or released to, the ECS undergoes a corresponding increase in its concentration (Rice and Nicholson, 1987). Diffusion can be effective for delivering soluble components to cells, with transport distances of the order of hundreds of micrometers, and is likely to be an efficient form of transport before extensive growth of the neurites, dendrites, and glial cells, and prior to the development of vascularization.

In this study, the glial currents were examined in brain slices, while the diffusion parameters were measured in the intact animal. The reason for performing the diffusion measurements in vivo is that the diffusion anisotropy would be impossible to study in thin slices, which are suitable for patch-clamp studies. However, the measurements of the ECS diffusion parameters show that there are no significant differences in the $\alpha$ and $\lambda$ values obtained in rat cortex in slices (Pérez-Pinzón et al., 1995) and in vivo (Lehmenkühler et al., 1993; Voříšek and Syková, 1997). This suggests that the differences in bathing solution and temperature in our experiments between the in situ slice and the intact rat do not invalidate our conclusions.

### Consequences for Spatial Buffering by Glial Cells

The driving force for spatial buffering of K$^+$ by glial cells is the difference between the membrane potential and K$^+$ equilibrium potential. Current flows inward where [K$^+$] is raised and outward elsewhere where [K$^+$] is low. The ''spatial'' current is driven by the membrane potential difference between regions of the glial syncytium. The process is facilitated by a low internal resistance, high membrane resistance, and selec-

tive permeability for K$^+$. Spatial buffering functions to equalize [K$^+$]$_e$ and prevent its local accumulation. The network of glial cells, coupled by low resistance gap junctions and K$^+$ selective membranes, is largely responsible for spatial buffering (Orkand et al., 1966; Coles and Orkand, 1983; Gardner-Medwin, 1983). In the paranodal regions, oligodendrocytes have intimate contacts with parts of the axonal membrane containing the highest concentration of potassium channels (Kocsis et al., 1986). A focal increase in [K$^+$]$_e$ after neuronal activity would induce spatial buffer K$^+$ currents at the paranodal loops. This would move K$^+$ into the oligodendrocyte at the area of the increase and out of the oligodendrocyte at distal parts. The efficiency of that process depends on the length constant of the oligodendrocyte membrane and the extent of electrical coupling to other oligodendrocytes or astrocytes (Massa and Mugnaini, 1982). Oligodendrocytes could be therefore highly efficient K$^+$ buffer elements in the myelinated tissue and in the corpus callosum. In the immature brain, the ECS is larger and there should be a greater ion flux across unmyelinated axons. Moreover, many of the precursor cells had a higher resistance to inward than outward current, whereas such rectification was lacking in the oligodendrocyte. It is therefore difficult to predict whether there will be more K$^+$ accumulation and spatial buffering in the corpus callosum of immature or mature animals. In gray matter of the spinal cord it was found that stimulation of dorsal roots increased [K$^+$]$_e$ more at P7 than in P14 and in adult animals (Jendelová and Syková, 1991).

### CONCLUSIONS

The membrane potential changes in mature oligodendrocytes which are produced by the activation of ionotropic receptors are accompanied by rapid changes in the K$^+$ gradient resulting from transmembrane K$^+$ fluxes. The K$^+$ fluxes produce larger changes in [K$^+$]$_e$ in the more mature myelinated corpus callosum than before myelination because the extracellular volume is less and the hindrance to diffusion is greater. The coincidence of the appearance of large K$^+$ tail currents in glial cells and the changes in extracellular diffusion parameters in the mature rat raise the question as to whether the decrease in volume and increase in tortuosity cause the increases in [K$^+$]$_e$. All of the results are consistent with such a conclusion. However, as the currents were studied in brain slices and the diffusion parameters in the intact animal and the geometry of the cells is so complex, it is not possible to make a quantitative comparison based on the independent measurements of the two phenomena. In addition, the diffusion measurements were made over a volume of the order of $10^{-3}$ mm$^3$, whereas the measurements of K$^+$ reversal potential consider the [K$^+$]$_e$ not in the bulk of the tissue but in the immediate vicinity of the

glial membrane. These considerations help account for differences between membrane currents in cells in slices or the intact brain compared to those in tissue culture where the ECS is essentially infinite.

## REFERENCES

Berger T, Schnitzer J, Kettenmann H (1991): Developmental changes in the membrane current pattern, K$^+$ buffer capacity and morphology of glial cells in the corpus callosum slice. J Neurosci 11:3008–3024.

Bjartmar C (1996): Oligodendroglial sheath lengths in developing rat ventral funiculus and corpus callosum. Neurosci Lett 216:85–88.

Bjartmar C, Hildebrand C, Loinder K (1994): Morphological heterogeneity of rat oligodendrocytes: Electron microscopic studies on serial sections. Glia 11:235–244.

Bondareff W, Pysh JJ (1968): Distribution of extracellular space during postnatal maturation of rat cerebral cortex. Anat Rec 160:773–780.

Chvátal A, Pastor A, Mauch M, Syková E, Kettenmann H (1995): Distinct populations of identified glial cells in the developing rat spinal cord: Ion channel properties and cell morphology. Eur J Neurosci 7:129–142.

Coles JA, Orkand RK (1983): Modification of potassium movement through the retina of the drone (*Apis mellifera*) by glial uptake. J Physiol (Lond) 340:157–174.

Connor JA, Stevens CF (1971): Voltage clamp studies of a transient outward membrane current in gastropod neural somata. J Physiol (Lond) 213:21–30.

Frankenhaeuser B, Hodgkin AL (1956): The after-effects of impulses in the giant nerve fibres of Loligo. J Physiol (Lond) 131:341–376.

Gardner-Medwin AR (1983): A study of the mechanisms by which potassium moves through brain tissue in the rat. J Physiol (Lond) 335:353–374.

Hamano K, Iwasaki N, Takeya T, Takita H (1996): A quantitative analysis of rat central nervous system myelination using the immunohistochemical method for MBP. Dev Brain Res 93:18–22.

Hamill OP, Marty A, Neher E, Sakmann B, Sigworth FJ (1981): Improved patch-clamp techniques for high-resolution current recording from cells and cell-free membrane patches. Pflügers Arch 391:85–100.

Hounsgaard J, Nicholson C (1983): Potassium accumulation around individual Purkinje cells in cerebellar slices from the guinea-pig. J Physiol (Lond) 340:359–388.

Jendelová P, Syková E (1991): Role of glia in K$^+$ and pH homeostasis in the neonatal rat spinal cord. Glia 4:56–63.

Kettenmann H, Sonnhof U, Schachner M (1983): Exclusive potassium dependence of the membrane potential in cultured mouse oligodendrocytes. J Neurosci 3:500–505.

Kettenmann H, Syková E, Orkand RK, Schachner M (1987): Glial potassium uptake following depletion by intracellular ionophoresis. Pflügers Arch 410:1–6.

Kocsis JD, Gordon TR, Waxman SG (1986): Mammalian optic nerve fibers display two pharmacologically distinct potassium channels. Brain Res 383:357–361.

Lehmenkühler A, Syková E, Svoboda J, Zilles K, Nicholson C (1993): Extracellular space parameters in the rat neocortex and subcortical white matter during postnatal development determined by diffusion analysis. Neuroscience 55:339–351.

Massa PT, Mugnaini E (1982): Cell junctions and intramembrane particles of astrocytes and oligodendrocytes: A freeze-fracture study. Neuroscience 7:523–538.

Nicholson C (1992): Quantitative analysis of extracellular space using the method of TMA$^+$ iontophoresis and the issue of TMA$^+$ uptake. Can J Physiol Pharmacol 70(Suppl):S314–S322.

Nicholson C, Phillips JM (1981): Ion diffusion modified by tortuosity and volume fraction in the extracellular microenvironment of the rat cerebellum. J Physiol (Lond) 321:225–257.

Nicholson C, Rice ME (1991): Diffusion of ions and transmitters in the brain cell microenvironment. In Fuxe K, Agnati LF (eds): "Volume Transmission in the Brain: Novel Mechanisms for Neural Transmission." New York: Raven Press, pp 279–294.

Orkand RK, Nicholls JG, Kuffler SW (1966): Effect of nerve impulses on the membrane potential of glial cells in the central nervous system of amphibia. J Neurophysiol 29:788–806.

Pérez-Pinzón MA, Tao L, Nicholson C (1995): Extracellular potassium, volume fraction and tortuosity in rat hippocampal CA1, CA3 and cortical slices during ischemia. J Neurophysiol 74:565–573.

Rice ME, Nicholson C (1987): Interstitial ascorbate in turtle brain is modulated by release and extracellular volume change. J Neurochem 49:1096–1104.

Rice ME, Okada C, Nicholson C (1993): Anisotropic and heterogenous diffusion in the turtle cerebellum: Implications for volume transmission. J Neurophysiol 70:2035–2044.

Sontheimer H, Kettenmann H (1988): Heterogeneity of potassium currents in cultured oligodendrocytes. Glia 1:415–420.

Sontheimer H, Trotter J, Schachner M, Kettenmann H (1989): Channel expression correlates with differentiation stage during the development of oligodendrocytes from their precursor cells in culture. Neuron 2:1135–1145.

Sturrock RR (1980): Myelination in the mouse corpus callosum. Neuropathol Appl Neurobiol 6:415–420.

Syková E (1991): Activity-related ionic and volume changes in neuronal microenvironment. In Fuxe K, Agnati LF (eds): "Volume Transmission in the Brain: Novel Mechanisms for Neural Transmission." New York: Raven Press, pp 317–336.

Syková E (1992): Ionic and volume changes in the microenvironment of nerve and receptor cells. In Ottoson D (ed): "Progress in Sensory Physiology 13." Heidelberg: Springer, pp 1–167.

Syková E (1997): The extracellular space in the CNS: Its regulation, volume and geometry in normal and pathological neuronal function. Neuroscientist 3:334–347.

Syková E, Svoboda J, Polák J, Chvátal A (1994): Extracellular volume fraction and diffusion characteristics during progressive ischemia and terminal anoxia in the spinal cord of the rat. J Cereb Blood Flow Metab 14:301–311.

Vernadakis A, Woodbury DM (1965): Cellular and extracellular spaces in developing rat brain. Arch Neurol 12:284–293.

Voříšek I, Prokopová Š, Syková E (1996): Diffusion anisotropy in white matter of the rat brain and spinal cord during development. Abstracts of the Second Conference of the Czech Neuroscience Society, Prague, p 74.

Voříšek I, Syková E (1997): Ischemia-induced changes in the extracellular space diffusion parameters, K$^+$ and pH in the developing rat cortex and corpus callosum. J Cereb Blood Flow Metab 17:191–203.